# The size-temperature "phase diagram" for small Lennard-Jones clusters.

Pavel A. Frantsuzov and Vladimir A. Mandelshtam
*Chemistry Department, University of California at Irvine, Irvine, CA 92697, USA*
(Dated: June 22, 2005)

The size-temperature "phase diagram" for small Lennard-Jones clusters $LJ_n$ ($n \leq 147$) is constructed based on the analysis of the heat capacities $C_v(T)$, computed by the Parallel Tempering Monte-Carlo method. Two types of "phase transitions" are often observed: the higher-temperature solid-liquid transition, due to melting of the cluster core, and the lower-temperature melting that occurs within the surface layer. The latter transition can only be observed for clusters with Mackay packing of the overlayer.

PACS numbers:

## Introduction.

Van der Waals interactions between rare gas atoms can be well described by the Lennard-Jones (LJ) potential,

$$u_{\rm LJ}(r) = 4\epsilon \left[ (r/\sigma)^{-12} - (r/\sigma)^{-6} \right], \qquad (1)$$

The possibility to compare the numerical results with experiments involving rare gas aggregates and the simplicity of the LJ potential placed the LJ systems among the most popular and most well studied. For last several decades they have played an important role in understanding the equilibrium and dynamics properties of liquids, solids and clusters. At the same time they were often used as benchmark systems for developing and testing new computational methods such as those designed for global optimization or for statistical mechanics calculations. For example, the Cambridge Cluster Database [1] gives putative global minima configurations for LJ clusters with sizes up to $n = 1000$. For each cluster size such calculation required substantial computational resources using state-of-the-art optimization algorithms.

The global minima describe only the zero-temperature equilibrium properties of clusters, while multiple local minima contribute to the cluster properties at finite temperatures. Various statistical mechanics techniques to characterize the finite temperature effects exist. Among those are the first-principles approaches, such as the Molecular Dynamics (MD) or Monte Carlo (MC), or approximate approaches, such as the superposition method (see, e.g., ref. [2]). For selected LJ clusters disconnectivity graphs providing information about the topology of the potential energy landscape in terms of the energies of local minima and transition states proved to be useful in characterizing their dynamics and equilibrium properties (see, e.g., ref. [3]).

Despite the long history until recently hardly any well converged MD or MC calculations were reported even for relatively small LJ clusters. One simple reason was the difficulty in attaining ergodicity in the LJ systems caused by the complexity of the potential energy landscapes with high dynamic ranges of the well depths and barrier heights. The real breakthrough was due to the adaptation of the parallel tempering method [4], allowing one to cope with the problem. The way it overcomes the high-energy barrier is by coupling a set of statistically independent Monte Carlo Markov chains via exchanges of configurations between replicas of slightly different temperatures. In the first successful application of the parallel tempering method to the challenging case of the $LJ_{38}$ cluster [5], in order to obtain a well converged heat capacity curve, as many as $10^{10}$ Monte-Carlo moves per temperature were required. While the main peak in $C_v(T)$ assigned to the solid-liquid transition converges very quickly, the real difficulty is associated with a correct description of the solid-solid transition showing up as a small bump in the $C_v(T)$ curve (see also refs. [6, 7]). The slow convergence in this particular case is mostly due to the long equilibration times needed to find multiple replicas of the global minimum that belongs to a narrow (octahedral) funnel of the potential energy landscape [3]. Although by setting the starting configurations to the global energy minimum reduces the equilibration times by about an order of magnitude, $10^9$ still seems large. Probably, the multifunnel nature of the $LJ_{38}$ is not an exclusion but rather typical property of most LJ clusters.

A later publication [8] which is a continuation of the previous study [9] reported well converged results of parallel tempering calculations for $LJ_n$ clusters up to $n = 60$. The existence of two peaks in the heat capacity curves was noted and extensively explored. Unfortunately in this study, no satisfactory explanation of the origin of the two peaks was given, while the focus was rather made on identifying the multiple "magic numbers" from the very detailed analysis of the structural and equilibrium properties as a function of $n$. Moreover, the existence of two distinct types of "phase transitions", as claimed in the present work, was not recognized. Here, in order to support our interpretation, we compute and analyze the heat capacity curves for $LJ_n$ clusters with sizes up to $n = 147$, i.e., up to the completion of the third overlayer.

TABLE I: The cluster sizes $n$, the constraining radii $R_c$, and the typical numbers of MC steps per temperature used in the present parallel tempering calculations for the four groups of clusters.

| Group | Sizes $n$ | $R_c/\sigma$ | $N_{\rm MC}$ |
|---|---|---|---|
| A | 10 - 40 | 2.5 | $1.5 \times 10^9$ |
| B | 20 - 57 | 3.0 | $2.0 \times 10^9$ |
| C | 50 - 80 | 3.5 | $1.25 \times 10^{10}$ |
| D | 80 - 147 | 4.0 | $1.25 \times 10^{10}$ |

### Parallel Tempering Calculations.

For each cluster size a parallel tempering calculation was carried out on a single processor. Except for not using parallelization, the present algorithm implementation was essentially identical to that described in ref. [5]. For all $n$ we implemented a hard constraining sphere with four different constraining radii for four different groups of clusters with overlapping size ranges as described in Table I. To reduce the computational burden for group D containing the largest clusters not all sizes were considered.

By recommendation of ref. [10] for an optimal temperature schedule we used a geometric sequence $T_i = T_{\rm min}\lambda^i$. The number of temperatures was varied from 20 to 40 depending on the cluster size and temperature range. For each $n$ the latter was chosen according to the expected nontrivial behavior of the $C_v(T)$ curve, ranging from temperatures as small as $T_{\rm min} = 0.01\epsilon k_{\rm b}^{-1}$ to $T_{\rm max} = 0.42\epsilon k_{\rm b}^{-1}$. The swaps of configurations between the random walks of adjacent temperatures were attempted every once in 100 MC steps per temperature, where one MC step corresponds to an attempt to move one of the atoms using the Metropolis scheme. In most cases the swap rates were about 50% or greater. However, at specific temperatures corresponding to large peaks in the heat capacity curves the swap rates could be noticeably below 50%. (Possibly, the overall convergence would be facilitated by the use of adaptive temperature grids [11].) Also, we took the advantage of the knowledge of the global minima configurations [1] and used them to set the initial configurations for all the random walks.

The heat capacities were computed using

$$C_v(T) = \frac{3nk_{\rm B}}{2} + \frac{1}{k_{\rm B}T^2}\left(\langle E^2\rangle_T - \langle E\rangle_T^2\right), \qquad (2)$$

In each parallel tempering calculation the energy moments $\langle E\rangle_T$ and $\langle E^2\rangle_T$ were partially averaged and written to the disk after every $N_{\rm MC} = 5 \times 10^7$ MC steps per temperature. In order to obtain smooth temperature-dependent observables for temperatures between the MC grid points they were calculated by the multi-histogram method [12, 13]. The convergence was monitored by comparing results obtained from independent runs. Once the comparison was favorable, the calculation was terminated. The typical (albeit not the largest) numbers of MC steps used in our calculations are shown in Table I. Generally, the convergence slows down with the increase of both the cluster size $n$ and the radius of the constraining sphere $R_c$. While it was easy to obtain converged results for the overall shapes of the heat capacity curves including the largest peaks, most time was typically spent to converge their small features. Our analysis indicates that with the given number ($\sim 10^{10}$) of MC steps for some clusters with $n \geq 100$ the heat capacities may not be well converged.

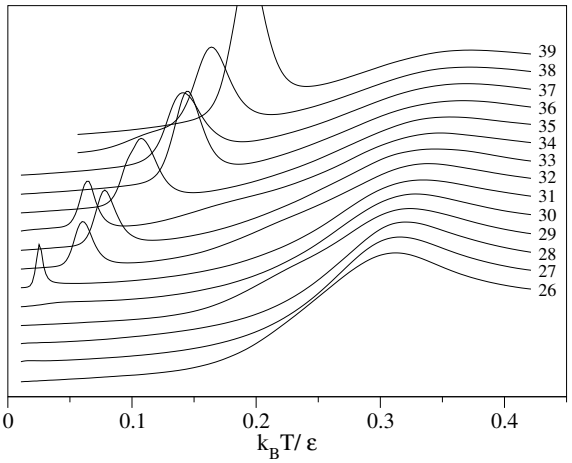


FIG. 1: Heat capacity curves $C_v(T)$ for a selected size range ($n = 26 - 39$) shifted along the y-axis for better visualization. The two peaks are clearly seen. The higher-temperature peak, caused by melting of the cluster core (resembling the structure of $LJ_{13}$), becomes less prominent with increasing $n$. The lower-temperature peak, due to the melting transition within the overlayer, increases in hight and shifts to the higher temperatures with more atoms in the overlayer.

### Results

Heat capacities for selected clusters are shown in figures 1 and 2. For each $n$ we estimated the temperatures at which the $C_v(T)$ curves have local maxima as shown in Fig. 3. For all cluster sizes considered $C_v(T)$ has at least one peak, while in many cases we observed two peaks. As can be seen from Fig. 1 for smaller clusters the higher temperature peaks are broad. Moreover, their shapes are sensitive to the constraining radius, so that the maxima observed for a particular $R_c$ may not be observed for a larger value of $R_c$ (see Fig. 3). However, for wide ranges of cluster sizes the two heat capacity peaks could be located unambiguously. A striking observation is that most peaks behave regularly as a function of $n$, which yields a simple interpretation.

The clusters with "magic numbers" of atoms, $LJ_{13}$,

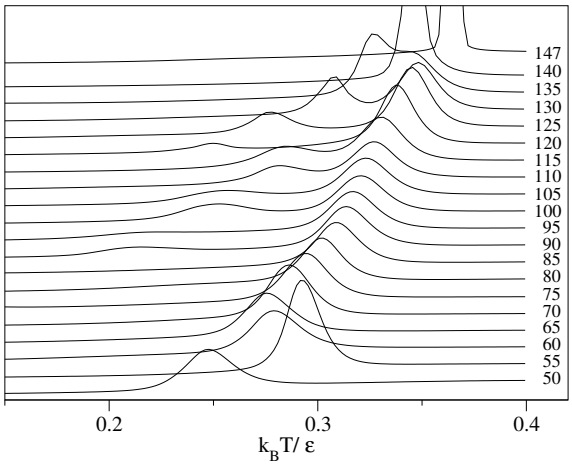


FIG. 2: Same as Fig. 1 but for a different range of cluster sizes $n$.

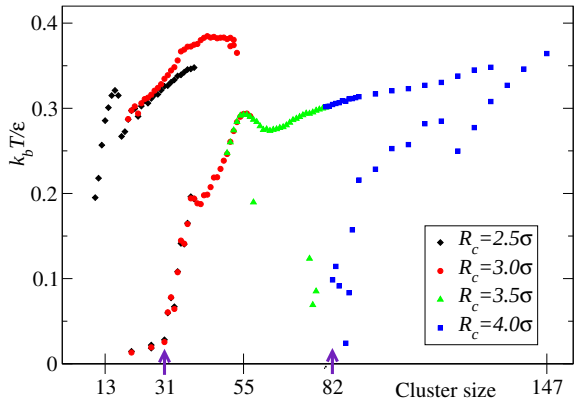


FIG. 3: Temperatures of the peak maxima of the $C_v(T)$ curves as a function of cluster size for four different values of the constraining radius, $R_c$. The positions of the higher-temperature peaks associated with melting of the cluster core ($LJ_{13}$) for sizes $25 \leq n \leq 53$ are sensitive to $R_c$. The arrows indicate the sizes (31,82) at which the Mackay packing of the overlayer becomes more preferable than the anti-Mackay packing at $T = 0$.

$LJ_{55}$ and $LJ_{147}$, form complete icosahedral structures and as such are most stable with respect to structural transformations. For most intermediate sizes, except a few cases (e.g., n=38,75,76,77), the equilibrium low temperature structure can roughly be represented as an icosahedral core with an incomplete overlayer [14–17]. For sizes $13 < n < 31$, $55 < n < 82$ and $n = 85$ the packing of the overlayer has the anti-Mackay structure, while for the other sizes with $n \geq 31$ and $\geq 82$ the overlayer structures are of the Mackay type [14–16]. While at least one peak in the $C_v(T)$ is observed for all sizes, the second, lower-temperature peak exists only for the clusters with Mackay overlayer. (Particularly, the second peak is not observed for $LJ_{85}$.) The exceptions are $LJ_{21}$ and $LJ_{27}$ with extremely small low-temperature peaks of unknown nature and $LJ_{58}$, $LJ_{75}$, $LJ_{76}$ and $LJ_{77}$. The second peak for $LJ_{58}$ is likely a result of relocation of the three atoms placed on the surface of the 55-atom icosahedral core, although it is not clear why similar effects are not observed for other sizes with anti-Mackay overlayer. The lower-temperature peaks for clusters with $n = 75, 76, 77$ with non-icosahedral global minima are due to the known solid-solid transition (see, e.g., ref. [2]) corresponding to global changes of cluster symmetry. A similar solid-solid transition occurs for $LJ_{38}$ [5], although it results in a bump, rather than a peak, in the $C_v(T)$ curve in addition to the two peaks of the general nature present in the other clusters with Mackay overlayer.

The above analysis unambiguously suggests that the lower-temperature peak for clusters with Mackay overlayer is due to the Mackay → anti-Mackay (M/aM) melting transition of the overlayer, while the higher temperature peak must be associated with the melting transition of the more stable icosahedral core. This interpretation is most clearly supported by Fig. 1 that shows the birth of the lower-temperature peak, at $n = 31$, which then rapidly increases in both the size and temperature. The Mackay-type packing becomes energetically more favorable when there are enough atoms in the overlayer, while the Anti-Mackay packing is more favorable entropically. This makes the latter to be thermodynamically dominant at higher temperatures and as such supports our interpretation of the lower-temperature melting as the M/aM transition. Note also that the two peaks merge for sizes around $n = 140$ with nearly complete overlayer, i.e., when the latter becomes especially stable. Furthermore, the tail from an adjacent peak may be relatively too large (e.g., for $n = 38$ or $n \geq 135$) resulting in a bump in $C_v(T)$ instead of a peak. All such bumps were ignored when constructing Fig. 3.

Although not based on converged calculations, evidences of surface melting in the LJ and other clusters were found and investigated previously [18–22]. Refs. [20, 21] explicitly attribute this transition for certain clusters to the M/aM type. Based on a well converged calculation for the special case of $LJ_{31}$ Calvo and Doye [23] demonstrated that the low temperature peak in the $C_v(T)$ curve does correspond to the M/aM transition.

In the present work we claim that the M/aM transition is generic for all clusters with Mackay overlayer. As the main evidence for this claim we use the behavior of the heat capacity peaks as a function of cluster size. A visual analysis (albeit not a quantitative proof) of cluster structures at different temperatures also supports our interpretation: For example, for clusters from Fig. 1 with $n \geq 31$ at temperatures below the low-temperature peak we observe nearly perfect global minima structures with Mackay packing in the overlayer. At temperatures between the two peaks we typically observe anti-Mackay

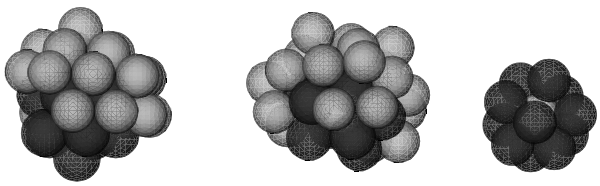

FIG. 4: Left: The global minimum configuration of $LJ_{35}$ with Mackay packing of the overlayer. Middle: Snapshot of $LJ_{35}$ at $T = 0.15\epsilon k_b^{-1}$, which is between the two heat capacity peaks. The melted overlayer resembles anti-Mackay packing. For the latter case 13 atoms that retain the complete icosahedral structure of $LJ_{13}$ can easily be identified (right).

packing with the cluster core retaining its icosahedral structure of $LJ_{13}$. The icosahedral core is destroyed only at substantially higher temperatures. For mere demonstration (but not prove) of our interpretation in Fig. 4 we show snapshots of $LJ_{35}$ in the two distinct regimes.

### Conclusions

In this paper we reported results of parallel tempering Monte Carlo calculations for LJ clusters for sizes $10 \leq n \leq 147$. We believe that for the temperature ranges considered the main features of the heat capacity curves are reproduced correctly, however there is a possibility that for some cases, particularly for $n \geq 100$, the convergence was not sufficient to make a clear judgment about the exact location of some peaks in the $C_v(T)$ curves. Only substantially more extensive parallel tempering calculations may clear this issue. However, independently of such possible errors, our results prove the existence of at least two qualitatively distinct solid-liquid-type transitions in the LJ clusters: a low-temperature M/aM transition within the overlayer, and the higher-temperature solid-liquid transition that occurs within the cluster core. These results are a manifestation of the complexity of the properties of finite systems (clusters) which is expected to disappear only in the bulk limit when the surface effects become relatively unimportant for equilibrium properties.

Besides involving larger clusters and certainly being more extensive, our further studies of LJ clusters will also consider other (than $C_v(T)$) equilibrium properties, such as appropriate spatial correlation functions, in order to gain more insight into the complexity of the phase transitions in these systems. Certainly, clever choices of the order parameters may significantly simplify the analysis.

Another interesting question emerging from this and previous studies is whether the quantum effects, due to the finite mass of the rare gas atoms, may change this picture. One step toward answering this question was made in ref. [7] where it was shown that the M/aM transition that occurs in the classical $LJ_{38}$ cluster does not occur in the quantum $Ne_{38}$ cluster, for which the ground state has the anti-Mackay, i.e, liquid-like, overlayer.

**Acknowledgment.** The NSF support, grant CHE-0414110, is acknowledged. V.A.M. is an Alfred P. Sloan research fellow. We are grateful to Florent Calvo for pointing our attention to some existing literature on surface melting and to Cristian Predescu for his comments on the parallel tempering procedure. Figure 4 was generated with VMD software package [24].

[1] http://www-wales.ch.cam.ac.uk/CCD.html
[2] J.P.K. Doye and F. Calvo *J. Chem. Phys.* **116**, 8307 (2002)
[3] J. P. K. Doye, M.A. Miller and D.J. Wales, *J. Chem. Phys.* **111**, 8417 (1999)
[4] C. J. Geyer, in *Computing Science and Statistics*: Proceedings of the 23rd Symposium on the Interface, ed. E. M. Keramigas, (Interface Foundation: Fairfax, 1991), pp. 156 - 163;
K. Hukushima and K. Nemoto *J. Phys. Soc. Jpn.* **65**, 1604 (1996).
[5] J. P. Neirotti, F. Calvo, D. L. Freeman, and J. D. Doll *J. Chem. Phys.* **112**, 10340 (2000);
F. Calvo, J. P. Neirotti, D. L. Freeman, and J. D. Doll *J. Chem. Phys.* **112**, 10350 (2000).
[6] D. Sabo, D.L. Freeman and J.D. Doll, *J. Chem. Phys.* **122**, 094716 (2005)
[7] C. Predescu, P.A. Frantsuzov and V. A. Mandelshtam, *J Chem. Phys.* **122**, 154305 (2005).
[8] D. D. Frantz, J. Chem. Phys. **115**, 6136 (2001).
[9] D. D. Frantz, J. Chem. Phys. **102**, 3747 (1995).
[10] C. Predescu, M. Predescu and C.V. Ciobanu, *J. Chem. Phys.* **120**, 4119 (2004).
[11] K. Hukushima and K. Nemoto, J. Phys. Soc. Jpn. **65**, 1604 (1996)
[12] A.M. Ferrenberg and R.H. Swendsen, *Phys. Rev. Lett.* **63**, 1195 (1989).
[13] P. Labastie and R.L. Whetten, *Phys. Rev. Lett.* **65**, 1567 (1990).
[14] J.A. Northby, *J. Chem. Phys.* **87**, 6166 (1987).
[15] J.P.K. Doye, D.J. Wales and R.S. Berry, *J. Chem. Phys.* **103**, 4234 (1995).
[16] R.H. Leary, *J. Global Optimization* **11**, 35 (1997).
[17] D.J. Wales and J.P.K. Doye, *J. Phys. Chem.* A **101**, 5111 (1997).
[18] H.-P. Cheng and R.S. Berry, *Phys. Rev.* A **45**, 7969 (1992).
[19] F. Calvo and P. Labastie, *Chem. Phys. Lett.* **258**, 233 (1996).
[20] J.P.K. Doye and D.J. Wales, *Z. Phys. D* **40**, 466 (1997).
[21] S.C. Hendy and B.D. Hall, *Phys. Rev. B* **64**, 085425 (2001)

[22] F. Calvo and F. Spiegelman, *J. Chem. Phys.* **120**, 9684 (2004).
[23] F. Calvo and J.P.K. Doye, *Phys. Rev.* E **63**, 010902 (2000).
[24] W. Humphrey, A. Dalke, and K. Schulten, *J. Molec. Graphics* **14**, 33 (1996).